CHEMISTRY OF MATERIALS

ARTICLE

pubs.acs.org/cm

Isomorphous Introduction of Boron in Germanosilicate Zeolites with UTL Topology

Oleksiy V. Shvets,*,† Mariya V. Shamzhy,† Pavel S. Yaremov,† Zuzana Musilová,‡ Dana Procházková,‡ and Jiří Čejka*,‡

†L.V. Pisarzhevskiy Institute of Physical Chemistry, National Academy of Sciences of Ukraine, 31 pr. Nauky, Kyiv 03028, Ukraine

‡J. Heyrovský Institute of Physical Chemistry, Academy of Sciences of Czech Republic, v.v.i., Dolejškova 3, 182 23 Prague 8, Czech Republic

Supporting Information

ABSTRACT: The direct introduction of boron into the framework of germanosilicate zeolites with UTL topology using different organic spiro azo compounds as structure-directing agents (SDAs) was performed. The influence of the SDA's nature, chemical composition and pH of the reaction mixture, and duration of the synthesis on the phase selectivity, limit of isomorphous introduction of boron into the zeolite framework and its location and coordination, and adsorption and acidic properties of prepared borogermanosilicates was investigated in detail. Experimental data provided clear evidence that the properties of the SDAs control the upper limit of the B content in the reaction mixture for successful synthesis of a pure UTL phase. UTL is formed in the pH region having the highest concentration of $Ge_8O_{15}(OH)_5^{3-}$ (D4R) in water. In synthesized UTL samples the contents of Si and Ge depend particularly on the pH values of the reaction mixtures with similar chemical compositions. With increasing pH of the reaction mixture, the silicon concentration increases, the germanium content predictably decreases, and the boron content shows a local minimum at pH ≈ 9. The concentration of boron in UTL samples is much less dependent on its content in the reaction mixtures. There is a sharp enhancement of the Si/Ge ratio in UTL samples synthesized from boron-rich reaction gels. A tentative assignment of ^{11}B magic-angle spinning NMR suggests that at lower contents of boron in the structure the boron atoms are located mainly in the T4 and T9 positions. With increasing pH above 11, a sharp increase in the Si/Ge ratio (decreasing the concentration of Ge atoms in D4R) was observed. It favors additional introduction of boron atoms into the T9 position. B-UTL zeolites contain predominantly Lewis acid sites with a small amount of Brønsted acid sites. The concentration of Brønsted acid sites sharply increases for samples prepared at pH lower than 8.

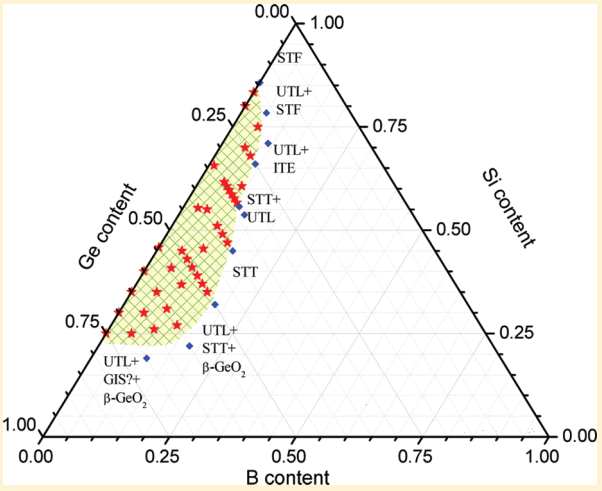

KEYWORDS: UTL zeolite, boron incorporation, structure-directing agent, role of pH, boron location

INTRODUCTION

Many new large-pore[1−5] and extra-large-pore[6−11] framework materials with previously unseen topologies have been successfully synthesized during the past decade in the system SiO_2/GeO_2 benefiting from a high flexibility of the Ge−O−Ge bond angle. It should be noted that successful synthesis of new extra-large-pore zeolites comprises utilization of optimum organic structure-directing agents (SDAs), appropriate synthesis conditions, and sometimes also the presence of inorganic structure directors.[6,9,11−14] The isomorphous incorporation of three-valent cations (e.g., Al, Ga, B, Fe) is a useful way to adjust the acidic properties of such materials.

Borosilicate zeolites display an acid strength significantly lower than that of the corresponding aluminosilicates but are still able to catalyze reactions such as double bond shift isomerization of linear olefins,[15] vapor-phase Beckmann rearrangement of cyclohexanone oxime to ε-caprolactam,[16,17] dehydration of cyclohexanol,[18] and reforming of FCC heavy gasoline and light cycle oil.[19] Borosilicates are also used in industrial processes such as the conversion of methyl *tert*-butyl ether to methanol and isobutene.[20] An advantage of B-ZSM-5 in comparison with Al-ZSM-5 for some special reactions such as double bond isomerization and aldehyde−ketone rearrangement[21] has been claimed. Using borosilicate zeolites significantly increased the yield of branched isomers C_6 in the conversion of *n*-hexane.[22]

Isomorphous introduction of boron into the framework of "traditional" zeolites was successful: MFI,[23−29] *BEA,[28,30−33] MEL,[24,25,34] MTW,[31,35] FER,[28,36,37] MWW,[38] EUO,[39] AFI,[28,40]

Received: January 13, 2011
Revised: March 29, 2011
Published: April 19, 2011

Table 1. Prepared Organic Compounds Used as SDAs in the Synthesis of Boron-Containing Germanosilicates[a]

N	SDA	C/N, 3°a + 4°a	pK_a	logP	N	SDA	C/N, 3°a + 4°a	pK_a	LogP
1		11, 2+1	12.40 ±0.03	−1.49 ±0.45	4		11, 1+1	12.30 ±0.03	−1.06 ±0.45
2		12, 2+1	12.19 ±0.03	−1.17 ±0.45	5		12, 1+1	12.15 ±0.03	−0.93 ±0.44
3		14, 2+1	11.86 ±0.03	−0.42 ±0.45	6		12, 2+1	11.84 ±0.04	−0.77 ±0.45

[a] In columns 3 and 8, "3°a + 4°a" indicates the quantity of ternary and quaternary atoms of C and N in a molecule of SDA.

CHA,[41] STF,[41,42] CON,[30,41,43−45] IFR,[30,46,47] ATS,[48] CAS,[49] ETBS-10.[50] Some new zeolite topologies were discovered as borosilicates (SFE,[51−53] SFH,[14] SFN,[14] SFS,[54] SFG,[55] SSY,[56] SSF,[57] MVY,[58,59]) or borogermanosilicate (IWR[60]).

Our previous investigation addressed the critical analysis of synthesis parameters of extra-large-pore germanosilicate with UTL topology, possessing 14-ring vs 12-ring pores.[61] (6*R*,10*S*)-6,10-dimethyl-5-azoniaspiro[4.5]decane hydroxide was used as the structure-directing agent. The kinetics of the synthesis, the role of the Si/Ge ratio in the synthesis mixture, and the effect of the calcination procedure were related to the crystallinity and textural properties of the synthesized zeolite. As a continuation of this investigation, the UTL germanosilicates have been synthesized using 13 spiro azo compounds as structure-directing agents.[62] The influence of the composition of the reaction mixture and template properties (structure, hydrophilicity/hydrophobicity, rigidity, pK_a) on the phase selectivity, crystallinity degree, and adsorption properties of UTL zeolites was investigated. Selection criteria of organic molecules as potential structure-directing agents for synthesis of large- and extra-large-pore zeolites from silicate and germanosilicate reaction media were proposed. We have shown clear synergism between the optimum structure of the organic template and the presence of a critical amount of inorganic component (GeO_2).

As a continuation of our research, we investigated a direct introduction of boron into the framework of germanosilicate zeolites with UTL topology using several spiro azo compounds, SDAs. The influence of the SDA's nature, chemical composition and pH of the reaction mixture, and duration of the synthesis on the phase selectivity, limits of isomorphous introduction of boron into the framework, location and coordination of boron atoms, and adsorption and acidic properties of prepared borogermanosilicates was investigated.

EXPERIMENTAL SECTION

Synthesis of the Templates. In general, preparation of SDAs was carried out using a method similar to that in ref 63 with subtle variations depending on the nature (primarily the solubility) of the obtained substances. Typically, 140 mL of distilled water, 5.68 g of sodium hydroxide, and 30.66 g of 1,4-dibromobutane (or an equimolar quantity of another bromo derivative) were mixed in a glass flask. A 16.07 g portion of (2*R*,6*S*)-2,6-dimethylpiperidine (or an equimolar quantity of another cyclic amine) was added dropwise over a period of 30 min under reflux. Then the mixture was refluxed under intense stirring (∼1000 rpm) for 12 h to prepare a milklike suspension and then cooled in an ice bath. After addition of 70 mL of an ice-cooled 50 wt % solution of sodium hydroxide, different quantities of solid sodium hydroxide were added under intense stirring and cooling by ice until an oil product appeared. As a rule, after 0.5−1 h of stirring, the oil crystallized, and the solid produced was filtered off and extracted with 100−500 mL amounts of chloroform. When no crystallization proceeded over an extended period of time, the reaction mixture was additionally cooled by means of liquid nitrogen, and the stark oil was separated mechanically. The organic fractions were dried by anhydrous sodium sulfate and partially evaporated, and the ammonium salt was precipitated and washed out with diethyl ether. Finally, the salts were converted into hydroxide form by ion exchange with Dowex SBR LCNG resin. The yield of the product, depending on the structure, was about 85−98%. The successful synthesis of the structure-directing agent was confirmed by ^{1}H NMR spectra after dissolution in dimethyl-d_6 sulfoxide. A list of all templates under study with their characteristics is given in Table 1.

Cyclic amines and bromo derivatives used for the synthesis of structure-directing agents: (2*R*,6*S*)-2,6-dimethylpiperidine, 3,5-dimethylpiperidine (mixture of *cis* and *trans*), decahydroquinoline (mixture of *cis* and *trans*), hexamethyleneimine, 2-ethylpiperidine, 1,4-dibromobutane, 1,5-dibromopentane, 1,4-dibromopentane. The compounds were prepared in pure forms as none of them are commercially available. Their structures were confirmed by ^{1}H NMR.[62] We measured the pH for 0.005−0.01 N mixtures of all obtained templates in their OH forms and used the data to calculate the experimental values of pK_a (presented in Table 1) as a degree of template basicity; for details see ref 62. Likewise, log *P* values (1-octanol/H_2O distribution coefficient, program ChemSketch 12.01) were calculated for characterization of the hydrophobicity degree of the templates. Calculation of the number of tertiary and quaternary atoms in the template skeleton as a measure of rigidity[64] was also carried out.

Preparation of the B-UTL zeolites was carried out using a method similar to that published in ref 62 with replacement of the silica source with H_3BO_3. The molar composition of the reaction mixtures was in the range $0.300-1.029SiO_2:0.0-0.156H_3BO_3:0.171-0.840GeO_2:0.2-0.7ROH/Br:30H_2O$. Typically, boric acid was dissolved in water with variable concentrations of SDA and hydroxide/bromide ratios. Then crystalline germanium oxide was added, and the mixture was stirred at room temperature until a clear solution was obtained. After this, silica (Aerosil 300) was added to the obtained solution, and the mixture was stirred at room temperature for 30 min. The resulting fluid gel was charged into 25 mL Teflon-lined autoclaves and heated at 175 °C for 2−23 days under agitation (∼25 rpm). Usually, for appropriate mixing of the reaction mixture, a small Teflon cylinder was inserted into the autoclave. The solid products obtained after preset synthesis times were recovered by filtration, washed out with distilled water, and dried

overnight at 95 °C. To remove the SDA, the as-synthesized zeolites were calcined in a stream of air at 550 °C for 6 h with a temperature ramp of 1 °C/min.

Characterization. X-ray powder diffraction data were obtained on a Bruker AXS D8 Advance diffractometer in the Bragg−Brentano geometry using Cu Kα radiation with a NaI dynamic scintillation detector. The relative crystallinity of individual zeolite samples was determined using the diffraction line at 6.23° with (*hkl*) index (200). To limit the effect of the preferential orientation of individual UTL crystals, a gentle grinding of the samples to decrease their size and careful packing into the holder were performed.

CHN analyses were carried out on a Carlo Erba 1106 analyzer.

The B, Si, and Ge contents were determined by elemental analysis. For this purpose 0.2−0.3 g of zeolite sample was heated at 70 °C with 5−7 mL of 10 M NaOH in a platinum cup. After total dissolution of the zeolite sample, 10−15 mL of concentrated HCl was added until the pH became 0.6−0.7, and the acid solution was evaporated at 50 °C for 1 h. Under these conditions Ge evaporated from the solution in the form of $GeCl_4$,[65] but volatilization of boron is slight (<3%). Then to the acidified residue was added 10−15 mL of concentrated HCl, and after 10 min 50 mL of hot water was also added. The precipitate was recovered by filtration on an ashless filter and washed out with acidulous distilled water and then with hot water for full removal of H_3BO_3. Precipitated $SiO_2 \cdot xH_2O$ was dried at 90 °C, calcined at 1000 °C until a constant mass was obtained, and weighed. The quantity of boron was determined by potentiometric titration of the filtrate. This muriatic solution of H_3BO_3 was neutralized until pH 6.95−7.05 was obtained with 5, 0.5, and 2×10^{-2} M NaOH sequentially. To the exactly neutralized solution was added 2 g of mannitol (a decrease of pH took place as a result of complexation of H_3BO_3 and mannitol), and titration was continued with 5×10^{-3} M NaOH until the pH returned to the original value of 6.95−7.05. The titer of NaOH was determined by potentiometric titration with a standard solution of oxalic acid.

For the quantitative determination of Ge in UTL zeolites, an alkaline solution of the samples (see above) was acidified with concentrated HCl until the pH value became ∼0.5, the precipitated SiO_2 was recovered by filtration, and Ge was determined in the filtrate by back-complexation titration using the following procedure. A 25.0 mL volume of 0.05 M EDTA was added to the analyzed solution, and the resulting solution was boiled for 10 min and then cooled and alkalized with 4 mL of a 25% aqueous solution of NH_3. The excess EDTA was titrated with 0.05 M $ZnSO_4$. The presence of B does not prevent chelatometric determination of Ge. All stages of this determination were tested on a model mixture of crystalline GeO_2, SiO_2, and H_3BO_3. The relative error of determination of each element did not exceed 5%.

The morphology of zeolite particles was evaluated using a scanning electron microscope, JEOL JSM-5500LV.

FTIR spectra of skeletal vibrations of UTL samples were recorded on an FTIR spectrometer, Spectrum One (Perkin-Elmer), using a KBr pellet technique.

The acidity of all zeolites was investigated by adsorption of pyridine and 2,6-di-*tert*-butylpyridine used as a probe molecule followed by FTIR spectroscopy.[66] Generally, studied zeolites were activated at 380 °C for 2 h. The adsorption of pyridine was carried out at 150 °C and investigated on a Spectrum One (Perkin-Elmer) spectrometer with a resolution of 1 cm^{-1}.

Adsorption isotherms of argon and nitrogen at −196 °C were measured with a Sorptomatic 1990 instrument. Prior to the adsorption measurements, all samples were degassed at 300 °C until a pressure of 0.001 Pa was obtained. Nitrogen or argon was used as the adsorbate to properly evaluate the pore size of this microporous germanosilicate. The micropore size distribution was calculated by using the Saito−Foley[67] method for cylinder pore geometry.

^{1}H NMR (300 MHz) spectra used for characterization of the structure-directing agent prepared were recorded on a Varian Mercury 300 spectrometer in dimethyl-d_6 sulfoxide solution at 25 °C (data are not shown here).

Solid-state ^{11}B magic-angle spinning (MAS) NMR spectra for selected samples were collected using a Bruker DSX-500 spectrometer (11.7 T) using a 4 mm cross-polarization magic-angle spinning (CPMAS) probe.

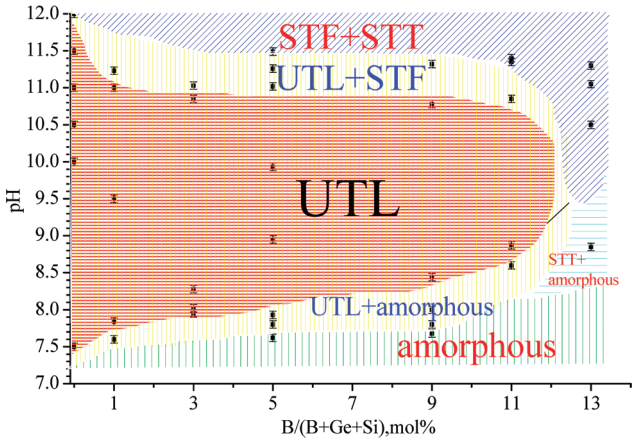

Figure 1. Influence of the pH and boron content in reaction mixtures on zeolite phase selectivity (175 °C, 10 days of synthesis, SDA4).

RESULTS AND DISCUSSION

On the basis of our recent results,[62] we selected a few SDAs which we found as the most favorable for the synthesis of UTL zeolite from B-free germanosilicate reaction mixtures. For the present study, reproducible formation of the UTL structure under a broad range of reaction mixture compositions and synthesis conditions (Si/Ge ratio, (Si + Ge)/SDA ratio, boron introduction, pH of the starting gel, duration of crystallization) was the crucial criterion for the selection. Hydrothermal synthesis in the presence of spiro azo compounds differing in structure and basicity (Table 1) as SDAs in borogermanosilicate reaction mixtures results in the formation of a pure phase of extra-large-pore UTL zeolites. Details of the typical synthesis are reported in Table SI-1, Supporting Information. For example, using SDA4 at a pH of the starting gel equal to 11 allowed UTL phase crystallization from the reaction mixture containing up to 11 mol % boron (Figure SI-1, Supporting Information). At higher concentrations of boron in the reaction mixture, we usually observed STF phase formation or an STF/STT mixture. For this series of B-UTL samples the calculated unit cell volume extremely decreased for ∼4 mol % boron in the reaction mixture (Figure SI-1, inset). In contrast to borosilicates, such compression of the unit cell parameter can be caused not only by decreasing the Si/B ratio but also by decreasing the Ge/Si ratio. This question is discussed in more detail vide infra on the basis of changes of the chemical composition for these samples.

We have investigated the influence of the pH value in B-containing germanosilicate reaction mixtures on the phase selectivity of zeolite formation. It should be noted that UTL crystallization is afforded in a wide range of pH (Figure 1). As for the crystallization of the B-free germanosilicate reaction mixture with SDA4, pure UTL phase is formed in the pH range from 7.5 to 11.5. When 1 mol % boron is added to the reaction mixture, the appropriate pH range is narrowed to 7.8−11.0, while for 9 mol % boron the range is diminished to 8.4−10.8 (Figure 1).

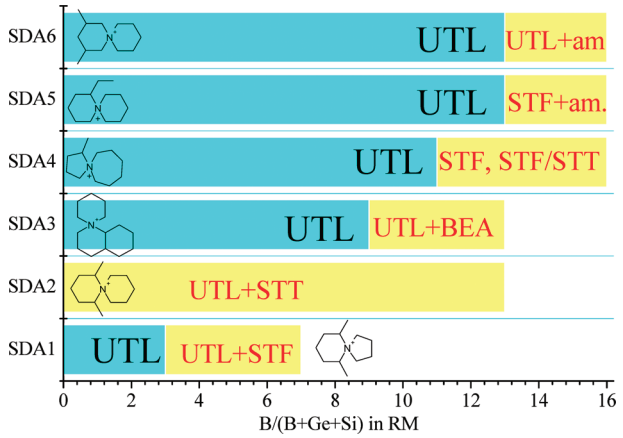

Figure 2. Influence of the SDA nature on zeolite phase selectivity in boron-containing germanosilicate reaction media (chemical composition and upper limit of B incorporation for represented zeolites indicated in Figure 3).

Enhancement of the pH in the reaction mixture also initiates the formation of the STF phase. Decreasing pH values caused essentially a prolongation of the crystallization, and at pH below 7.5 we did not observe any zeolite phase to be formed when using SDA4. For extremely long crystallization times, mixtures of tridimite, α-quartz, and β-GeO_2 were obtained. Increasing the boron content to 13 mol % at pH 8−9.3 led to the formation of the STT phase.

SDAs used in this study have a sufficiently high hydrolytic stability. The pH of the reaction mixtures significantly increased during the synthesis due to the release of OH^- groups due to a condensation of silicate, germanate, and borate anions in the crystallization process. In the case of templates with a lower hydrolytic stability (Beckmann rearrangement partially occurs in some tertiary amines), we noted a slight increase in pH during the crystallization.

The properties of SDAs strongly influence the upper limit of the B content in the reaction mixture, still providing pure UTL phase. Syntheses using SDA4, SDA5, and SDA6 resulted in the formation of a pure UTL phase in a wide range of B/(Si + Ge + B) ratios from 0.1 to 11 (Figure 2). In contrast, with SDA1 the UTL phase is formed only up to 3 mol % boron in the reaction mixture. When higher concentrations of B were used, a mixture of UTL with STF was formed. Synthesis in the presence of SDA2 in borogermanosilicate media led to the formation of UTL only in a mixture with STT in the whole range of boron content studied. SDA3 occupies an intermediate position among these templates: the still acceptable maximum of the boron content in the reaction mixture for UTL formation is 9 mol %. At higher boron content and pH > 12, we observed formation of *BEA zeolite.

Seemingly, the size and shape of the SDAs along with their basicity and balance of hydrophobicity/hydrophilicity are important features of organic cations controlling the phase selectivity of zeolite formation from a B-containing reaction mixture. SDA4, SDA5, and SDA6 have very similar structure selectivities: a close limit of acceptable content of boron in the reaction mixture and formation of the STF phase behind this limit. SDA1 predictably shows a fast enough transition to zeolites with STF topology. It is caused, probably, by a significant decrease in the energy of the molecule with its location in the "barrel" cavity in the channel of the STF structure at formation in aluminosilicates or borosilicate reaction mixtures in the presence of SDA1.[68] Using SDA3 in high silica media usually resulted in crystallization of SSZ-31 zeolite[69] with *STO topology. We could not obtain a pure UTL phase (only UTL/STT mixtures) from borogermanosilicate reaction mixtures with SDA2. This is especially surprising when considering that in the presence of SDA2 the UTL structure easily crystallizes from a pure germanosilicate medium or after introduction of indium(III) or iron(III) sources into the reaction mixture.

As shown in ref 67, UTL zeolite can be prepared from B-free germanosilicate reaction mixtures with a great variety of SDAs. These SDAs should only satisfy the stability under the synthesis conditions, balance of hydrophobicity/hydrophilicity, etc.[70] Obviously, the SDAs used are not specific stabilizers of the void region within the UTL framework against dissolution and transformation to denser, more stable phases. It is known that piperidinium derivatives of such nature, size, and shape are good stabilizers for more dense zeolite framework (STF, ITE, and STT depending on other synthetic conditions) when working in borosilicate reaction media.[71] Therefore, from the thermodynamic point of view, if the denser phase (in this case STF or STT) is more stabilized by a given SDA, then we should expect the denser phase to be preferably formed under all conditions. Nevertheless, most molecules are selective for the UTL phase over a wide range of reaction mixture compositions. This is due to the presence of Ge in the reaction mixture playing the key role in the UTL crystallization process as UTL is formed from borosilicate sheets and preferable germanate D4R building units.

D4R secondary building units (SBUs) are the important part of the UTL structure as they expand silica sheets in a pillar-like fashion, forming 14-ring pores. Ge atoms preferentially occupy positions in D4R, thus stabilizing the structures.[72]

The aqueous chemistry of solutions of germanium dioxide provides some explanation of pH borders for UTL formation. Cotton and Wilkinson reported that major ionic species in diluted aqueous solutions of GeO_2 appear to be $Ge(OH)_3O^-$, $Ge(OH)_2O_2^{2-}$, and $Ge_8O_{15}(OH)_5^{3-}$.[73] According to ref 74, the germania solution phase diagram consists of three distinct regions: region I (pH > 11.4) containing germania monomers $Ge(OH)_3O^-$, region II (7.4 < pH < 11.4) containing octamers in equilibrium with soluble germania (Everest and Salmon[75,76] reported that if the germanium concentration in water solution is higher than 0.01 M in the pH range 6.9−9.4 only the germanium ion is a singly charged ion—pentagermanic acid, $HGe_5O_{11}^-$), and region III (0 < pH < 7.4) containing octamers, soluble germania, and condensed and/or aggregated germania particles. Thus, $Ge_8O_{15}(OH)_5^{3-}$ species playing a significant role in UTL formation (D4R) exist in the pH range 0−11.4. Initially, when the pH decreases to ∼10, the total amount of $Ge_8O_{15}(OH)_5^{3-}$ increases, but as the pH is lowered, there is a mixture of octameric species present in solution with varying degrees of deprotonation.[74] In addition, the solubility of GeO_2 and hence the concentration of octameric species in region III (0 < pH < 7.4) are probably not sufficient for stabilization of the UTL framework. Therefore, the pH border of UTL formation is equal to the pH limits of region II with the highest concentration of $Ge_8O_{15}(OH)_5^{3-}$ (D4R) species.

If the final structure grows around these D4R units, then structures containing D4R units will be favored over those not containing them.[77] Burton et al.[71] showed that SDA1, which we use for synthesis of UTL samples, is particularly selective for

zeolites with large cage structures (such as STT, STF, and ITE) due to the strong correlation between the shape and size of an SDA molecule and the cage sizes of these zeolites and hence strong van der Waals interactions between the SDA and the zeolite framework. It may be assumed that other SDAs (e.g., 2, 4, 5, 6) used in this work are also good stabilizers for more dense large-cage-structure zeolite frameworks, as their kinetic diameters differ only slightly from that of SDA1. Thus, UTL and denser large-pore zeolites will be competitive phases in germanosilicate reaction mixtures containing such SDAs. When the relative concentration of $Ge_8O_{15}(OH)_5^{3-}$ (D4R) in the reaction mixture is high (pH 7.4−10, poor silicate mixtures), UTL is the primary phase. With decreasing concentration of $Ge_8O_{15}(OH)_5^{3-}$, the stabilization energy of UTL decreases and STF (STT, ITE) becomes a more thermodynamically favored phase.

The investigation of the influence of the substitution of silicon for germanium in aqueous prenucleating and nucleating solutions of tertiary amine hydroxide by the electrospray ionization mass spectrometry method was published recently.[78] The obtained results demonstrated that independently of the organic template nature (TMAOH, TEAOH, or TPAOH) the major species observed in the synthesized prenucleating solutions were single 4R and D4R units. The authors also noted that increasing the template concentration in the reaction mixtures led to an increase in the degree of germanosilicate species polycondensation. We believe that this is due to an increase in the pH of the solutions and, consequently, a change in the balance of dissolution/deposition of silica and germanium dioxide (nucleation species become more silicated). We note another experimental observation of this work:[78] with increasing softness of the templates as a base, the degree of polycondensation increases; in particular the dominant particle in solution becomes D4R.

The formation of acid−base pairs is highly probable in B-containing reaction mixtures and has been demonstrated by different authors in the case of B-MFI zeolites.[29,47] The stability of $(B-O-Si)^-SDA^+$ ion pairs increases with increasing Lewis acid softness of SDA cations.[79] The Lewis acid softness of SDAs used in this paper increases in the order SDA6 < SDA5 ≈ SDA4 < SDA1 < SDA2. Most likely, the order of the SDA stabilization energy for cage-type zeolite formation increases in the same direction, as the size of the SDA molecule approximates the best fit of van der Waals interactions between the SDA and the zeolite framework. Thus, the introduction of a boron source into the reaction mixture results in the appearance of centers of crystallization (ion pairs of SDA^+ with large borosilicate anions) of large-cage (cavity) zeolites competing with D4R building units. SDA1 has a high STF stabilizing energy[71] and in cationic form is a soft Lewis acid. Probably in a similar way the SDA2/STT system also has a high stabilizing energy. This results in parallel crystallization of the mixture of the STT phase and is provoked by the presence of even a moderate quantity of B−O−Si species. SDA4, SDA5, and SDA6 have relatively low stabilization ability for STF or STT formation compared to SDA1 or SDA2 and $(B-O-Si)^-SDA^+$ ion pair stability. This is why the UTL phase has energetic preference until the B concentration in the reaction mixture reaches 13 mol %.

The increase in the boron content in the reaction mixture causes enhancement of the amount of B−O−Si species and consequently the probability of formation of more thermodynamically stable dense phases. This effect can be compensated with increasing concentration of $Ge_8O_{15}(OH)_5^{3-}$ building blocks, changing the pH value. We have noted that the highest concentration of $Ge_8O_{15}(OH)_5^{3-}$ is at pH ≈ 10. As a result, with increasing B content in the reaction mixture, the lower limit of UTL formation shifts toward higher pH values (7.4 → 10.0) and the upper limit shifts toward lower pH values (11.4 → 10.0).

The chemical composition of the samples with UTL topology crystallized from different reaction mixtures changes in a wide range. Some general tendencies can be observed in Figure 3 and Table 2.

(a) The content of organic components (based on thermogravimetric and CHN analyses) in highly crystalline UTL samples changes in the range 11.5−13.8 wt %, the C/N ratio in the analyzed series of UTL samples is approximately constant and is equivalent to ∼11 in the case of SDA4, and the H/N ratio is close to 22. These data confirm inclusion of SDAs in the channels of the zeolites and, mostly, preservation of an organic template in the cationic form without any decomposition.

(b) As for borosilicates, the boron content in UTL samples crystallized from a low-alkaline germanosilicate reaction mixture (pH 8.9−9.1), as well as from a high-alkaline reaction mixture (pH 11.1−11.4), is practically constant and does not depend straightforwardly on its content in the reaction mixtures (0.5−0.4 mol % for low pH and 0.9−1.0 mol % for high pH accordingly). In contrast, the silicon content substantially increases and the germanium content decreases with increasing boron concentration in the reaction mixture. Consequently, there is a sharp enhancement of the Si/Ge ratio (especially at pH 11.1−11.4) for samples synthesized from boron-rich gels.

These results are in contrast with those of other borosilicates having a boron content proportional to its contents in the respective reaction mixture, although crystallization of a boralite often requires a large excess of boron in the synthesis gel with respect to the amount really incorporated into the crystalline product.[23] This might be related to a poor stability of the boron atom in the framework, escaping easily from the framework even after its incorporation.

Theoretical calculations show that the formation of Si−O−Me bridges is energetically more favorable than the formation of Si−O−Si.[80] This is reflected in the precipitation of metal hydrosilicates during dissolution of a complex silicate.[81] The calculated distribution[82] of Ge and Si species as a function of pH at 25 °C and at saturated pressure of water in germanosilicate solution without SDA shows transformation of half of $Ge(OH)_4$ into $GeO(OH)_3^-$ at pH ≈ 9.3 and half of $Si(OH)_4$ into $SiO(OH)_3^-$ at pH ≈ 9.8. At 250 °C these two critical points shift to pH ≈ 8.4 and 8.9 (due to the shift neutrality point of water from pH 7 to pH ≈ 5.6). For UTL we witness the greatest change in the Si/Ge ratio in samples prepared in the pH range from 7.5 to 9.5, which is in agreement with these data. Simultaneously, it should be considered that the differences between the thermodynamic properties of $Ge(OH)_4^0(aq)$ and $Si(OH)_4^0(aq)$ species ($\Delta_f H^\circ_{298}$ and $C^\circ_{p,298}$ are equal to −346.2 kcal/mol and −40 cal mol^{-1} K^{-1} and −267.0 kcal/mol and −50 cal mol^{-1} K^{-1}, respectively) increase with the Ge/Si ratio and temperature in aqueous solutions in equilibrium with Ge-bearing silicates.[82]

In the case of borogermanosilicates, formation of species $B(OH)_3$, $SiO(OH)_3^-$, $Si_4O_8(OH)_4^{4-}$, and $Ge_8O_{15}(OH)_5^{3-}$ shall be considered. During the condensation of these units, at first nucleophilic attack on the boron nucleus should proceed since the B−OH group of the borate ion is much less nucleophilic than the $Si-O^-$−group and especially the $Ge-O^-$−group. Thus, formation of Si−O−B species is

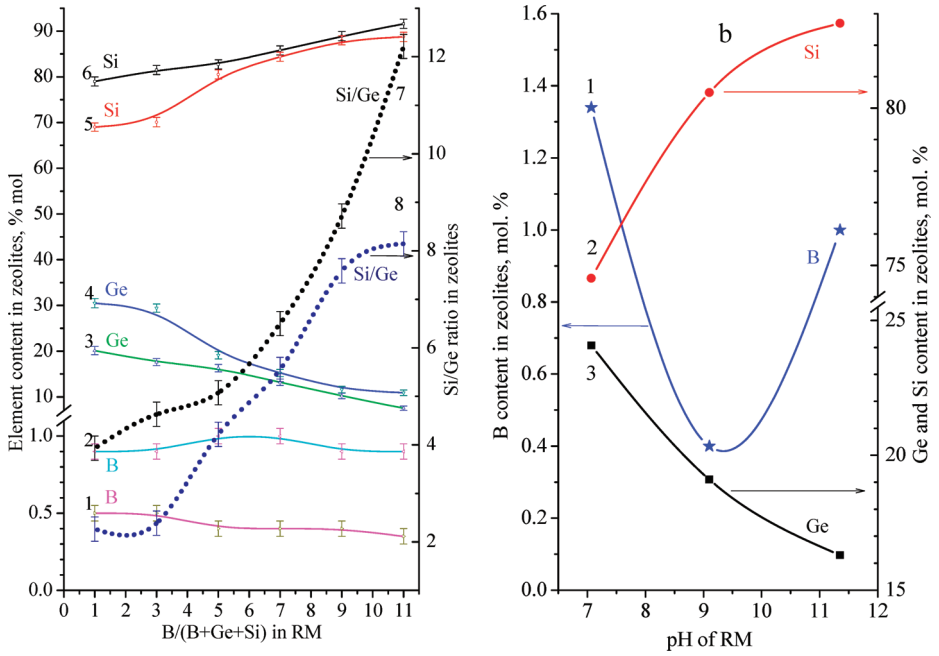

Figure 3. Dependence of the framework composition of UTL samples on the B content in the reaction mixture and pH value (175 °C, SDA4, SDA5, and SDA6): (a) (1) B, (4) Ge, and (5) Si contents and (8) Si/Ge ratio for series zeolite samples prepared at pH 8.9−9.1; (2) B, (3) Ge, and (6) Si contents and (7) Si/Ge ratio for series zeolite samples prepared at pH 11.1−11.4; (b) (1) B, (2) Si, (3), and Ge contents in samples prepared from reaction mixtures with B:Si:Ge:SDA = 0.06:0.74:0.4:0.5 and different pH values.

Table 2. Study of the Effect of Changing the Initial B Concentration and pH Value during UTL Synthesis in the Presence of SDA4

			framework composition, mol %				organic template	
sample	B/(B + Ge + Si) in reaction mixture	pH of reaction mixture	B	Ge	Si	B/(B + Ge + Si)	[C], wt %	[N], wt %
B-UTL-4-5	0.05	11.00	1.0	16.3	82.7	0.010	10.53	1.01
B-UTL-4-9	0.07	10.94	1.0	13.2	85.8	0.010	10.14	0.98
B-UTL-4-12	0.09	11.32	0.9	10.2	88.9	0.009	10.86	1.02
B-UTL-4-14	0.11	11.35	0.9	7.5	91.6	0.009	9.92	0.90

probably followed by the formation of Si−O−Ge. Competition of Ge and B for condensation with silicate species and primary formation of Si−O−B species results in a decrease in the Ge content in UTL zeolites.

(c) For a series of UTL zeolites prepared from reaction mixtures with similar chemical compositions and different pH values, the B, Si, and Ge contents extremely depend on the pH value. While the silicon content increases and the germanium content predictably decreases with pH, the boron content shows a local minimum at pH ≈ 9.

Such a dependence of the B content in UTL samples on the pH in the reaction mixture can be explained considering the boron anion distribution in solution and mechanism of B−O−Si species formation. When investigating the hydrothermal condensation mechanism of B-containing zeolite with MFI structure, de Ruiter et al.[26,83] proposed that the framework was built by the condensation of silicon building units with boron units through the boron nuclei were nucleophilically attacked by $Si-O^-$ groups. As tetrahedrally coordinated boron species, $B(OH)^-_4$, cannot form the 5-coordinated sp^3d transition state required for S_N2-type reaction, it cannot be condensed with the $Si-O^-$ group; only the $B(OH)_3$ building unit can react.

Boric acid has a water solubility of 57 g/L and does not dissociate in aqueous solution as a Brønsted acid but as a Lewis acid interacting with water molecules to form the tetrahydroxyborate ion.[84] Adding OH^- to a boric acid ($B[OH]_3$) solution starts with boric acid's solubility curve, but as the pH increases, pentaborate (isolated $[B_5O_6(OH)_4^-]$) is formed exhibiting comparatively high solubility. In the pH range 7−10, tetraborate ($B_4O_5(OH)_4^{2-}$) is next formed with a medium solubility for boron concentrations higher than about 0.025 mol/L. As for pH higher than about 10, metaborate species ($B[OH]_4^-$) are present and are highly soluble. At pH 7 the concentration of $B(OH)_3$ species capable of condensation with $Si-O^-$ fragments is high, which is why we can observe maximal B content in UTL samples. At pH 9 the concentration of tetraborate anions is maximal and results in a decrease in the B content in the solid product. At pH 9−11 the tetraborate anion concentration in solution decreases, so the B content in zeolite slightly increases. At pH > 11.5 all soluble boron species are in the form of $B(OH)_4^-$ and are not capable of reacting with $Si-O^-$ species. Thus, at higher pH a very low content of boron is found in the solid samples.

In the case of borogermanosilicates, condensation and crystallization processes are somewhat complicated due to the presence

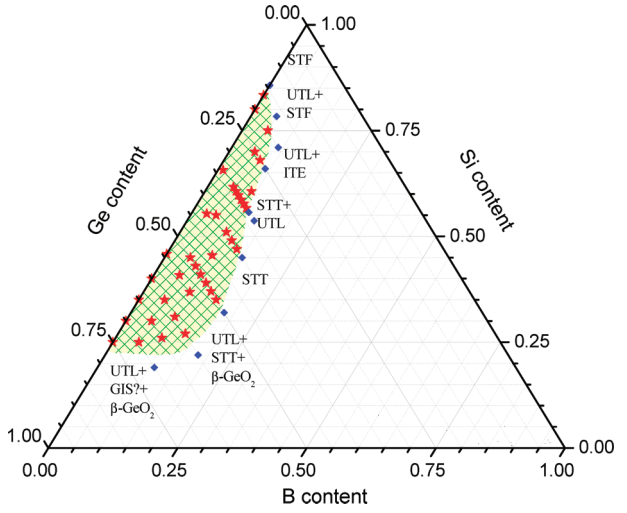

Figure 4. Phase diagram depicting the products obtained as a function of the reaction mixture composition (pH 10.9−11.2, 175 °C, 2−23 days of synthesis, SDA5).

of dissolved germanium in the reaction mixture. In the investigated pH range the solubilities of compounds of boron, germanium, and silicon in water differ significantly. Silica solubility is practically pH-independent (120−138 mg/L) at pH < 9, but increases dramatically with increasing pH at pH > 9 (180, 310, 876, and ∼5000 mg/L at pH 9.5, 10.0, 10.6, and 10.8, respectively).[85] The solubility of amorphous silica in water at the vapor pressure of the solution at pH 8 increases almost linearly with increasing temperature and at 175 °C reaches values of 850−900 mg/L.[86] At pH < 8, the main species in an aqueous solution of silica is H_4SiO_4. At concentrations higher than 110−140 mg/L SiO_2 and pH > 6.5, polymerization takes place, yielding polysilicic acids and a colloid, gel, or precipitate.[87] $Si_4O_8(OH)_6^{2-}$ is dominant in solution at pH 9, $Si_4O_8(OH)_4^{4-}$ (and partially $SiO(OH)_3^-$) at pH 10−12, and $SiO_2(OH)_2^{2-}$ at pH > 13.[88]

The increase in the relative content of silica and the decrease in the Ge content in UTL samples synthesized in the pH range 7−10.6 are caused by sharply increasing Ge dissolution, whereas the solubility of silicon is still very low under these conditions. GeO_2 solubility is practically constant only until pH 7.5. From this value every increase in pH in steps of 1 results in a 10-fold increase in the Ge solubility. Under the conditions of the hydrothermal synthesis, the GeO_2 solubility increases with pH (extremely beginning from 8.7), which is consistent with the dissociation of germanic acid.[88]

Whereas aluminosilicates can be synthesized at high Al^{3+} and OH^- concentrations ($OH^-/Si > 0.50$), most borosilicates will not crystallize at all owing to favorable solubilization of both silicates and borates above pH 11. Aluminates are less soluble at high pH values, and therefore, crystallization of aluminosilicates is favored under these conditions.[45] Reaction mixtures for synthesis of zeolites with UTL topology investigated in this study have $OH^-/(Si + Ge + B)$ ratios in a range of ∼0.05−0.41 and pH 7.07−12.88. Crystallization of borogermanosilicate phases at relatively low $OH^-/(Si + Ge + B)$ but at high pH (>11) can be explained as follows: The pH value of the reaction mixture is overestimated and characterizes the concentration of free OH^- ions in the interparticle aqueous media. Whereas sources of germanium and boron totally dissolve in SDA−OH solution, silica sources (Cab-O-Sil M5 or Aerosil 380) form a fluid gel, allowing the crystallization of such zeolites at high enough pH. Using an equimolar quantity of a silica source (for example, TEOS) for such synthesis significantly decreases the pH value of the reaction mixture. During hydrothermal synthesis the pH usually increases due to the release of OH^- ions at polycondensation of hydroxides.

It is necessary to note that the majority of "successful" syntheses of zeolites with UTL topology proceeded in reaction mixtures with the $OH^-/(Si + Ge + B)$ value in the range 0.05−0.34 (see Table SI-1, Supporting Information). The only exception is SDA3, for which we found appropriate values of $OH^-/(Si + Ge + B)$ up to 0.41. The maximum allowable $OH^-/(Si + Ge + B)$ value depends on the composition of the reaction mixture: an increase in the Si/Ge ratio in the gel not only improves the upper limit of the latter but also requires an increase in lower acceptable values. In the reaction mixture with a low boron concentration, a wide range of $OH^-/(Si + Ge + B)$ values are appropriate; at 9−11 mol % B, this range usually narrows to 0.11−0.22.

Zeolites with UTL topology can crystallize from the reaction mixtures with a wide variability of chemical compositions (Figure 4). A detailed study of the peculiarities of crystallization of this zeolite phase shows that for a B-free reaction mixture at pH ≈ 11.0, the acceptable contents of germanium and silicon are 0.167−0.750 and 0.833−0.250, respectively. In a silicon-rich reaction medium, we observed the beginning of the formation of the STF phase but with some decrease in pH and the appearance of tridimite. For Ge-rich reaction media, the rapid emergence of the β-GeO_2 impurity is typical. The successful synthesis of UTL zeolites from so different reaction mixtures requires very substantial control of the duration of hydrothermal synthesis, which is due to dramatic changes in the crystallization kinetics. At Si/Ge = 5 in the reaction mixture, the optimum time of the hydrothermal synthesis is 15−17 days, whereas at Si/Ge < 0.66 it is only 2 days. Introduction of boron into the reaction mixture requires some prolongation of the crystallization. When the boron content increases to 11% at constant Ge content, the average prolongation of the crystallization time is 1.6−1.8-fold. Although usually borosilicates crystallize much more rapidly than silicates or aluminosilicates,[52] in the presence of germanium this tendency is reversed. Increasing the boron content in the reaction medium narrows the fields of appropriate contents of silicon and germanium (Figure 4). Typical impurities in the samples obtained from relatively boron rich reaction mixtures using SDA5 are STF, STT, and ITE. In the case of other SDAs, other phases such as *BEA, MFI, MEL, and MTW can be formed. It should be noted that, by changing the pH of the reaction mixture, the region of UTL phase existence changes significantly. With a decrease in pH to 9 the β-GeO_2 phase was observed already at a Si/Ge ratio equal to 1, while at a high Si/Ge ratio the β-GeO_2 phase does not occur. At pH above 12, the region of existence of the UTL phase is restricted to Si/Ge values from 1.5 to 3.

Scanning electron microscopy (SEM) images of UTL zeolites prepared using SDA5 in the reaction mixture at pH ≈ 11.2−11.9 showed similar homogeneous sheetlike crystals with a thickness of less than 0.2 μm and an average size of about 4 × 4 μm (Figure SI-2, Supporting Information). The majority of crystals are isolated ones, while the minority of them consist of aggregates of lamellar crystals. It should be noted that SEM together with powder X-ray diffraction (XRD) confirms a high degree of

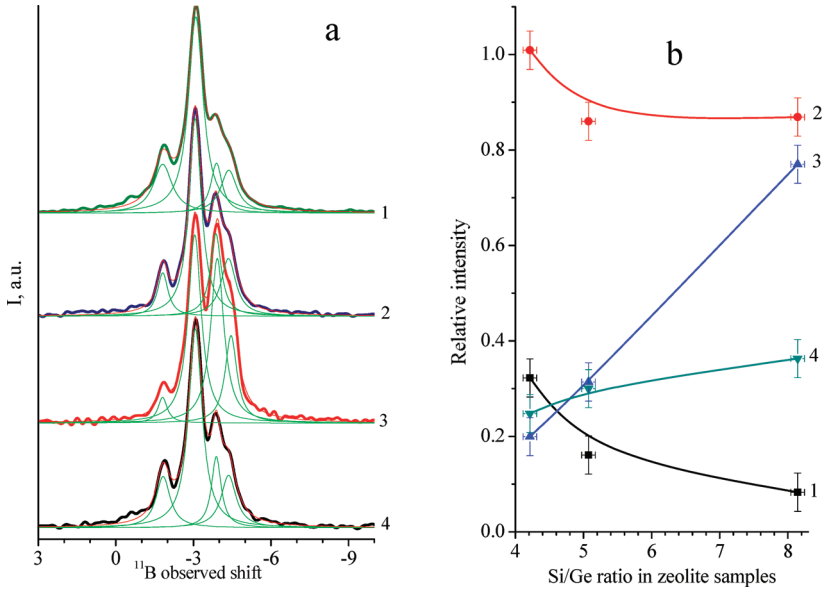

Figure 5. (a) ^{11}B MAS NMR spectra of as-synthesized B-UTL zeolite samples: (1) B-UTL-4-3, (2) B-UTL-4-14, (3) B-UTL-4-8, (4) B-UTL-4-15. (b) Dependence of the intensity of the peaks on the Si/Ge ratio: (1) −1.86 ppm, (2) −3.08 ppm, (3) −3.89 ppm, (4) −4.39 ppm.

crystallinity and phase purity of the prepared samples of UTL zeolites. The resulting morphology of the crystals under study differs from the morphology of IM-12 crystals described by Paillaud et al.[7] The authors reported on the formation of two types of crystals: large aggregates with a size of 150 × 150 × 150 μm under static synthesis conditions and flower-type aggregates of thin crystals under agitation. The morphology of the crystals also differs from that published previously due to the differences in the synthesis conditions.[62]

^{11}B MAS NMR Data. ^{11}B MAS NMR spectra of four as-synthesized B-UTL zeolite samples are shown in Figure 5a. Decomposition of the spectra can be made with high accuracy on four Lorenz components with resonances of −1.86 ± 0.01, −3.08 ± 0.02, −3.89 ± 0.03, and −4.39 ± 0.03 ppm, accordingly. For some samples we can also see a low-intensity shoulder at −0.67 ± 0.05, probably indicating the presence of a negligible amount of trigonal BO_x units. ^{11}B MAS NMR data clearly evidence that in freshly prepared UTL zeolites all boron atoms have a tetrahedral environment and they are a part of a zeolite framework. Different shifts of BO_4 probably caused differences in the nature of the nearest T neighbors (Si, Ge), combined with the presence of B in different crystallographic sites. Many authors reported that the position of the peak in a ^{11}B MAS NMR spectrum of tetrahedral boron in the framework can change in a wide range from −1.3 for MCM-70(MVY)[54] to −3.6 ppm for B-MTW,[35] −4.0 ppm for B-*BEA,[30] and −4.5 for SSZ-42-(IFR)[47] depending on the type of zeolite structure and the chemical nature of the coordination environment.

To try to localize boron atoms in the UTL zeolite structure, we have analyzed the changes of the intensities of all four peaks depending on the Si/Ge ratio in the studied samples (Figure 5b) and the pH of crystallization (Table SI-1, Supporting Information). As evident from Figure 5b, the intensity of the peak at −3.89 ppm continuously increases with increasing Si/Ge ratio. In contrast, the intensity of the peak at −1.86 ppm constantly decreases with increasing Si/Ge ratio. On this basis, we assume that these two peaks can be attributed to boron atoms in the positions of the UTL structure with one Ge atom and three Si atoms in the first coordination sphere. For peaks at −3.08 and −4.39 ppm such dependence of their intensity is not straightforward as the intensity correlates with the total content of boron in the samples. It follows from this fact that the last two peaks could be assigned to boron atoms located in different framework positions in a completely silica environment.

For specification of the possible boron location in the UTL framework, we used the results of a previously theoretical investigation.[89] The authors report on calculations on the substitution of silicon or germanium in T11 and T12 sites for aluminum, boron, or gallium in the cluster of the UTL structure. Calculated substitution energies using the DFT-LDA and the DFT-GGA approximations for 10 nonequivalent T sites testifies that isomorphous introduction of trivalent elements in some positions is possible. Substitution energies increase in the order T4 < T6 < T9 ≈ T5 ≈ T1 ≪ T2 ≈ T7 < T8 ≪ T11 ≈ T12. The authors excluded positions T3 and T10 from consideration assuming the isomorphous silicon replacement in these positions is impossible.

Germanium atoms in the UTL structure are preferably located in the T11 and T12 positions (D4R), especially for samples having high Si/Ge ratios. Hence, the presence of one germanium atom at the first coordination sphere of the boron atom is possible only for the T9 site among the first five energetically most favored crystallographic positions in the UTL structure. In this case, the peak at −3.89 ppm could probably correspond to a boron atom located in the T9 position with a completely silica environment, whereas the peak at −1.86 ppm can be attributed to boron atoms in the T9 position with one germanium atom in the nearest neighborhood. The most intense peak at −3.08 ppm can be attributed to atoms in the energetically most favorable T4 position and the peak at −4.39 ppm to atoms in position T6. For the last two positions a completely siliceous environment is most likely. From ^{11}B MAS NMR data it can be assumed that at rather low contents of boron in the structure of zeolites (prepared from reaction mixtures with a relatively low pH of 8−9) the boron atoms are located mainly in the T4 and T9 positions and at a lesser extent in position T6. The increasing pH

dx.doi.org/10.1021/cm200105f |*Chem. Mater.* 2011, 23, 2573–2585

of the reaction mixture above 11 leads to a sharp increase in the Si/Ge ratio (and a decrease in the Ge atom content located in D4R) in zeolite samples and favors the additional introduction of boron atoms in the T9 position. It is also necessary to notice that T atoms in the T4 and T6 positions of the UTL structure are connected to the common oxygen atom (O19) while the simultaneous presence of two boron atoms is forbidden by the Löwenstein rule. This reduces 2-fold the total amount in these positions. In a similar way, T atoms in the T9 and T6 positions are also connected to the common oxygen atom (O22). Such a geometry of the UTL structure creates preconditions for introduction of a 2-fold higher amount of boron atoms in the T9 and T4 positions instead of the T6 position, especially for high-silica-containing samples.

FTIR Spectroscopy Data. FTIR spectra in the framework vibration region of calcined UTL samples of B-containing germanosilicate are shown in Figure SI-3, Supporting Information. In the spectrum of pure germanosilicate zeolite several IR bands are observed: structure-insensitive bands at 1084, 782, and 440 cm^{-1}, which are common for all silicate materials, and structure-sensitive bands at 1240, 877, 660, 582, and 524 cm^{-1}. A shoulder in the spectrum found at ~1000 cm^{-1} (980 cm^{-1} in the as-synthesized sample) and a weak band at 940 cm^{-1} could be assigned to Si−O vibrations in different Si−O−Ge moieties. The band at 877 cm^{-1} and weak shoulder at 820 cm^{-1}, most likely, can be attributed to an asymmetrical stretching vibration of Ge−O of the tetrahedrally coordinated germanium, whereas the band at 582 cm^{-1} can be attributed to the symmetrical stretching vibration of Ge−O.[90]

For B-containing germanosilicate samples with UTL topology, additional IR bands at 1453, 1384, and 908 cm^{-1} and a doublet at 794 and 759 cm^{-1} appeared in the spectra. The bands at 1384 and 908 cm^{-1} correspond to asymmetric and symmetric vibrations of the B−O bond in the B−O−Si group, where the boron is a trigonally coordinated framework boron[91,92] practically in all borogermanosilicates samples. The absorption band at 1384 cm^{-1} is observed only in H-form zeolites because this peak is very sensitive to sorption of basic adsorbates. A new absorption band at 1453 cm^{-1}, as far as we know, was not observed earlier for B-containing zeolites. Taking into consideration the chemical composition of this zeolite sample and also the ^{11}B MAS NMR data, it would be possible to attribute this band to asymmetric vibrations of the B−O bond in the B−O−Ge group, where the boron is located in the framework position T9. The bathochromic shift of ν_{OTO} caused by the introduction of boron or other atoms into the framework has been reported by many authors.[23] We also observed a shift of the band at 1084 cm^{-1} to 1077 cm^{-1}, which testifies to incorporation of boron into the UTL structure. Among other changes in the FTIR spectra, it is necessary to note the disappearance of the band at 660 cm^{-1} for samples synthesized from a high-pH reaction mixture, splitting of the band at 782 cm^{-1} into a pair of bands at 794 and 759 cm^{-1} for the zeolite samples synthesized from a low-pH reaction mixture, and the disappearance of the shoulder at 1000 cm^{-1} for all B-containing germanosilicates with UTL topology.

Adsorption Data. Textural parameters of the porous structure of the B-UTL zeolites were determined using adsorption isotherms with nitrogen as the adsorbate (Figure SI-4 and SI-6, Supporting Information). The Brunauer−Emmett−Teller (BET) areas were in the range 500−610 m^2/g. The micropore volume of crystalline zeolite samples prepared with different SDAs agrees well with the total amount of template and water in as-synthesized samples (DTA + TG and CHN analysis data) and was on average 0.19−0.23 cm^3/g.[62] The variation in the pore volume ((0.23 − 0.19)/0.23 × 100) is probably due to the presence of some traces of nonporous solids (amorphous) or a difference in the crystallinity degree.

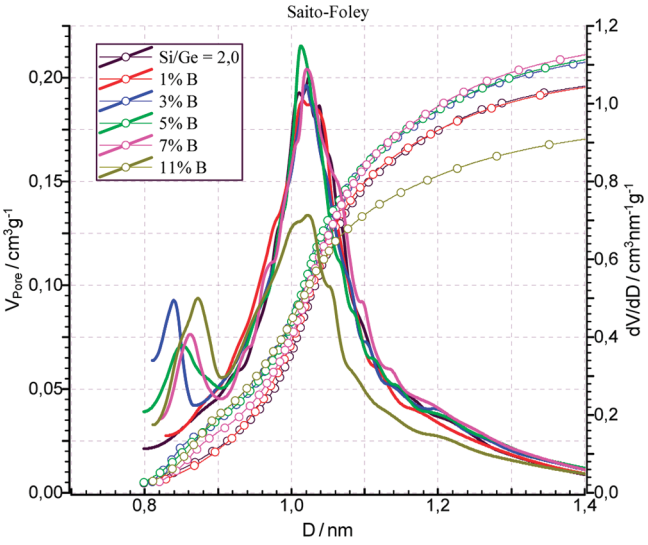

Figure 6. Micropore size distribution for samples of B-UTL zeolite prepared with use of SDA5 from reaction mixtures with different contents of boron.

The analysis of N_2 adsorption isotherms in the pressure range (p/p_0) from 10^{-6} to 10^{-3} allowed determination of the micropore size distributions for calcined samples. For the determination based on the nitrogen adsorption isotherm Saito−Foley[93] method, the average pore diameter was estimated close to 1.05 nm. We note that the value obtained from nitrogen measurements is somewhat higher than that from crystal structure data. It is important to note that in micropore size distributions for some samples two maxima have been obtained. N_2 adsorption data have shown a clear dependence of the pore size distribution on the quantity of boron in the reaction media (Figure 6). In particular, with increasing boron content (more than 3 mol %), the narrowed (~0.84−0.86 nm) pores increased.

To check our hypothesis, we measured the adsorption isotherms of argon as a nonpolarizable atom (Figure SI-5, Supporting Information). Analysis of Ar adsorption isotherms evidences the identical pore size distribution. This result shows that in this case there has been a real change in the size of some of the channels. We believe that the most probable reason is changing of the 12- and 14-ring pore geometry due to framework distortion. This distortion could be due to the replacement of germanium atoms in a certain positions in the D4R for silicon atoms. This changes the O−T−O and T−O−T angles, and the 12-ring channels become more elliptic. Similar changes were observed for germanosilicate zeolites with UTL topology and Si/Ge ratios of more than 10 in solid samples. It should also be noted that for the relatively Ge rich (probably Si/Ge ≈ 4) UTL zeolites (IM-12)[7] the authors present the distribution of pore sizes with a maximum at 10.5 Å, while in high-silica (probably Si/Ge > 14) UTL zeolites (ITQ-15)[6] the maximum is 7.5 Å.

Acidity of B-UTL Samples. Pyridine adsorption on B-UTL zeolite usually indicates predominantly a Lewis acid sites and a small amount of Brønsted acid sites (Figure 7a). Only for

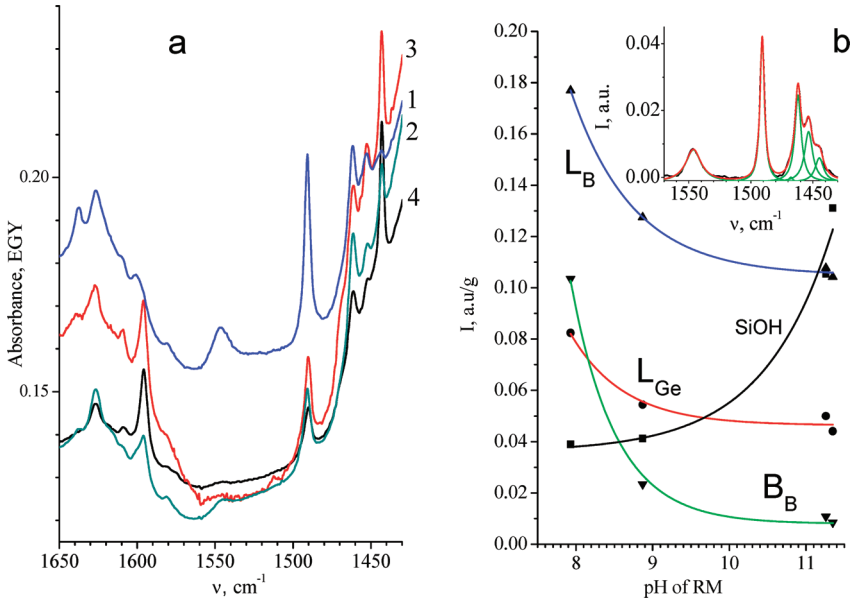

Figure 7. (a) FTIR spectra of pyridine adsorbed on B-UTL zeolite synthesized from reaction mixtures of different compositions: (1) B-UTL-4-3, (2) B-UTL-4-14, (3) B-UTL-4-3, (4) B-UTL-4-15. (b) Dependence of the acidity distribution (bands at 1542 cm^{-1} (B_B), 1452 cm^{-1} (L_{Ge}), and 1462 cm^{-1} (L_B)) for B-UTL zeolite on the pH value of the reaction mixtures.

samples prepared at pH less than 8 does the concentration of the Brønsted acid sites (bands at 1542 and 1638 cm^{-1}) increase sharply. As follows from Figure 7a in the UTL borogermanosilicates, several types of Lewis acid centers are present: in the range 1430−1475 cm^{-1} we observed three bands at 1443, 1452, and 1462 cm^{-1} and sometimes a shoulder at 1470 cm^{-1}. The band at 1443 cm^{-1} could be attributed H-bonded pyridine coordinated to silanol groups.[94] The second band and bands at 1609 and 1622 cm^{-1} are tentatively assigned to pyridine adsorbed on four-coordinated germanium atoms.[95] The intensity of these bands correlates with the Si/Ge ratio in the samples. For pure germanosilicate zeolites this band (1452 cm^{-1}) is present in the spectra, and its intensity changes in parallel with increasing Si/Ge ratio in the reaction mixture at constant pH or with elevation of the pH with identical Si:Ge:B:SDA ratio in the reaction mixture. The band at 1462 cm^{-1} was observed only in B-UTL samples, and its intensity generally depends on the boron content in the samples. However, it should be noted that, for each sample studied, the relative intensities of the bands at 1462 and 1542 cm^{-1} depend on the evacuation conditions before adsorption of pyridine. The temperature threshold of stability in a vacuum fo 5×10^{-3} Torr for the bridged OH groups associated with boron is 370−380 °C. This temperature is quite sufficient to completely remove adsorbed water molecules from B-UTL zeolites and to achieve a residual pressure of 5×10^{-3} Torr. At higher temperatures of activation we observed a partial destruction of the bridged OH groups. As a consequence, reduction in the intensity of the absorption band at 1542 cm^{-1} and growth of the band at 1462 cm^{-1} (as well as at 1638 cm^{-1}) were found. At temperatures above 450−470 °C most of these Si−O(H)−B groups are destroyed, and obviously the boron atoms are transformed into the three-coordinated state. There is no clear relationship between the boron concentration in the reaction mixture and the intensity of the "boron" absorption bands of adsorbed pyridine. We also observed an absorption band at 1609 cm^{-1}, the intensity of which correlates with the intensity of the band at 1443 cm^{-1}. In particular, the band is more intense in high-silica UTL zeolites synthesized from the reaction mixtures at a higher pH. The assignment of the absorption band at 1608−1609 cm^{-1} to pyridine coordinated to the germanium species could be proposed.[96]

It looks like the relative and absolute intensities of the bands of pyridine adsorbed on Brønsted and Lewis acid sites are influenced by the pH values of the reaction medium. As can be seen from Figure 7b, increasing the pH from ∼8 to ∼9 leads to a very substantial decrease in the number of Brønsted acid sites as well as to the reduction of the concentration of Lewis acid sites. In the same pH range, the concentration of Lewis acid sites attributable to the atoms of the four-coordinated germanium[95] is reduced to a lesser extent, whereas the concentration of Si−OH groups remains practically unchanged. These results are in agreement with the above-described results on the effect of the pH of the reaction mixture on the boron content and Si/Ge ratio in the samples of UTL zeolites. An increase in the pH above 11.2 causes a sharp increase in the concentration of silicon defects, which obviously reflects a very substantial increase in the Si/Ge ratio in the samples. In this case, the concentration of Lewis acid sites attributed to the atoms of the four-coordinated germanium slightly decreased. We observed some reduction of the concentration of "boron" acid centers of both types, although the results of chemical analysis show that the boron concentration in the samples increases slightly. Apparently, the reduction of the concentration of boron centers could be related to an increase in boron removal from the framework by calcination.

Compared with aluminosilicate zeolites, borosilicates always show a lower acidity (weaker acid sites). Our results of ammonia temperature-programmed desorption (TPD) showed that the strength of the acid sites for borogermanosilicate zeolites with UTL topology differs little from that of the nonacidic surface: in addition to the peak at 195 °C, we observe only a weakly expressed shoulder at 220 °C.

Last but not least, another feature of germanosilicate UTL zeolite is mentioned. In the hydrated state, at least part of the

Table 3. Amount of Accessible Acid Sites (Si/B) and Type and Concentration of Brønsted and Lewis Acid Sites Determined after Adsorption of 2,6-Di-*tert*-butylpyridine

sample	B/(B + Ge + Si) in reaction mixture	pH of reaction mixture	Si/B (FT-IR)	c_B (mmol/g)	c_{Br} (mmol/g)	c_{Le} (mmol/g)	c_{Br} (%)	c_{Le} (%)
B-UTL-5-8	5	11.86	39.2	0.42	0.02	0.20	10	90
B-UTL-5-31	10	11.64	37.2	0.44	0.02	0.21	11	89
B-UTL-5-35	11	11.44	39.1	0.42	0.01	0.21	4	96
B-UTL-5-39	12	11.28	29.9	0.54	0.02	0.26	6	94

germanium atoms coordinate water molecules to form donor−acceptor complexes. When sample evacuation is carried out at 250 °C, coordinated water molecules are retained in the pores, whereas most of the water is removed. Adsorbed pyridine "recognizes" polarized water molecules coordinated with germanium as Brønsted acid sites: the spectrum contains a fairly intense absorption band at 1542 cm^{-1}, while the band at 1452 cm^{-1} remains very low. Heating of the samples above 350 °C in vacuum leads to the removal of water complexes from framework germanium atoms. As a consequence, in the spectrum of adsorbed pyridine, the band at 1542 cm^{-1} is practically not observed while another band appears at 1452 cm^{-1}, the intensity of which correlates with the content of germanium in the zeolite samples.

To determine the effect of the boron content in the germanosilicate reaction mixtures with a high pH on the concentration and type as well as the availability of acid sites, we also studied the adsorption of 2,6-di-*tert*-butylpyridine.[66] Similarly to pyridine adsorption on B-UTL zeolite, adsorption of 2,6-di-*tert*-butylpyridine shows predominantly Lewis acid sites (three types) and a small amount of Brønsted acid sites (Figure SI-6, Supporting Information). In the OH group region, the absorption band at 3663 cm^{-1} disappeared after 2,6-di-*tert*-butylpyridine adsorption. For a series of samples synthesized from reaction mixtures with a pH value of more then 11, the concentration of Brønsted centers is almost independent of the boron content in the reaction mixture (Table 3, Figure 7b). The concentration of boron in the samples (determined from the position of Si−O absorption bands in the FTIR spectra) increases slightly with increasing concentration of boron in the reaction mixture, which is reflected in the increasing concentration of Lewis acid sites. Some overestimation of the Si/B value may be due to the presence of germanium atoms of the zeolite framework, which slightly increases the average distance of T−O.

CONCLUSION

The properties of SDAs strongly influence the upper limit of the B content in the reaction mixture, which still allows pure UTL phase to be obtained. The pH borders of UTL formation are equal to the pH limits of the region where the concentration of $Ge_8O_{15}(OH)_5^{3-}$ (D4R) in water is the highest. For a series of UTL samples prepared from reaction mixtures with similar chemical compositions and different pH values, the B, Si, and Ge contents extremely depend on the pH value. While the silicon content increases and the germanium content predictably decreases with pH increments, the boron content shows a local minimum at pH ≈ 9. The boron content in the UTL samples does not depend straightforwardly on its content in the reaction mixtures, but the silicon content substantially increases and the germanium content decreases with increasing amount of boron in the reaction mixture. Consequently, there is a sharp enhancement of the Si/Ge ratio for samples synthesized from boron-rich reaction gels. From ^{11}B MAS NMR data it probably follows that at rather low contents of boron in the structure of zeolites (prepared from reaction mixtures with a relatively low pH of 8−9) the boron atoms are located mainly in the T4 and T9 positions and in a smaller extent in position T6. The increasing pH of the reaction mixture above 11 leads to a sharp increase in the Si/Ge ratio (and a decrease in the concentration of Ge atoms in D4Rs) and favors additional introduction of boron atoms in the T9 position. B-UTL zeolites exhibit predominantly Lewis acid sites and a small amount of Brønsted acid sites. Only for samples prepared at pH lower than 8 does the concentration of the Brønsted acid sites increase sharply.

ASSOCIATED CONTENT

Supporting Information. Figures showing the XRD patterns and SEM image of B-containing samples, FTIR spectra of skeletal vibrations of B-UTL zeolites, adsorption isotherms of nitrogen for samples of B-UTL zeolite, micropore size distribution for samples of B-UTL-5−35, and IR spectra of the hydroxyl vibration region of UTL and a table giving the details of the most representative synthesis of UTL zeolite. This material is available free of charge via the Internet at http://pubs.acs.org.

AUTHOR INFORMATION

Corresponding Author

*E-mail: alexshvets@ukr.net (O.V.S.); jiri.cejka@jh-inst.cas.cz (J.Č.).

ACKNOWLEDGMENT

J.Č. and D.P. thank the Grant Agency of the Czech Republic for the financial support of this study (Grants 203/08/0604 and P106/11/0819). We thank Dr. J. Dědeček for recording the B NMR spectra.

REFERENCES

(1) Corma, A.; Navarro, M. T.; Rey, F.; Rius, J.; Valencia, S. *Angew. Chem., Int. Ed.* **2001**, *40*, 2277.
(2) Corma, A.; Díaz-Cabanas, M. J.; Martínez-Triguero, L. J.; Rey, F; Rius, J. *Nature* **2002**, *418*, 514.
(3) Corma, A.; Rey, F.; Valencia, S.; Jordá, J. L. *Nat. Mater.* **2003**, *2*, 493.
(4) Cantín, A.; Corma, A.; Díaz-Cabanas, M. J.; Jordá, J. L.; Moliner, M. *J. Am. Chem. Soc.* **2006**, *128*, 4216.
(5) Dorset, D. L.; Strohmaier, K. G.; Kliewer, C. E.; Corma, A.; Díaz-Cabanas, M. J. *Chem. Mater.* **2008**, *20*, 5325.
(6) Corma, A.; Boulahya, M. J. D. *Chem. Commun.* **2004**, 1356.
(7) Paillaud, J. L.; Harbuzaru, B.; Patarin, J.; Bats, N. *Science* **2004**, *304*, 990.
(8) Corma, A.; Moliner, M. J. D. *Nature* **2006**, *443*, 842.
(9) Sun, J. L.; Bonneau, C.; Cantin, A.; Corma, A.; Diaz-Cabanas, M. J.; Moliner, M.; Zhang, D. L.; Li, M. R.; Zou, X. D. *Nature* **2009**, *458*, 1154.

(10) Jiang, J.; Jorda, J. L.; Diaz-Cabanas, M. J.; Yu, J.; Corma, A. *Angew. Chem., Int. Ed.* **2010**, *49*, 4986.
(11) Corma, A.; Díaz-Cabanas, M. J.; Jiang, J.; Afeworki, M.; Dorset, D. L.; Soled, S. L.; Strohmaier, K. G. *Proc. Natl. Acad. Sci. U.S.A.* **2010**, *107*, 13997.
(12) Freyhardt, C. C.; Tsapatsis, M.; Lobo, R. F.; Balkus, K. J., Jr.; Davis, M. E. *Nature* **1996**, *381*, 295.
(13) Wagner, P.; Yoshikawa, M.; Lovallo, M.; Tsuji, K.; Taspatsis, M.; Davis, M. E. *Chem. Commun.* **1997**, 2179.
(14) Burton, A.; Elomari, S.; Chen, C. Y.; Medrud, R. C.; Chan, I. Y.; Bull, L. M.; Kibby, C.; Harris, T. V.; Zones, S. I.; Vittoratos, E. S. *Chem.—Eur. J.* **2003**, *9*, 5737.
(15) Hölderich, W. *Stud. Surf. Sci. Catal.* **1986**, *28*, 827.
(16) Roeseler, J.; Heitmann, G.; Hölderich, W. F. *Appl. Catal.* **1996**, *114*, 319.
(17) Roeseler, J.; Heitmann, G.; Hölderich, W. *Stud. Surf. Sci. Catal.* **1997**, *105*, 1173.
(18) Brabec, L.; Novakova, J.; Kubelkova, L. *J. Mol. Catal.* **1994**, *94*, 117.
(19) Chen, C. Y.; Zones, S. I. *Stud. Surf. Sci. Catal.* **2001**, *135*, 159.
(20) Taramasso, M.; Manara, G.; Fattore, V.; Notari, B. GB Patent 2,024,790, 1990.
(21) Marosi, L.; Stabenow, J.; Schwarzmann, M. EP 7 081, EP 46 504, EP 10 572.
(22) Abramova, A. V.; Slivinskii, E. V.; Matieva, Z. M.; Kitaev, L. E.; Yushchenko, V. V.; Kubasov, A. A.; Tkachenko, O. P. *Pet. Chem.* **2000**, *40*, 248.
(23) Millini, R.; Perego, G.; Bellussi, G. *Top. Catal.* **1999**, *9*, 13.
(24) Shilun, Q.; Wenqin, P.; Shanqing, Y. *Stud. Surf. Sci. Catal.* **1989**, *49*, 133.
(25) Simon, M. W.; Nam, S. S.; Xu, W.; Suib, S. L.; Edwards, J. C.; O'Young, C. *J. Phys. Chem.* **1992**, *96*, 6381.
(26) de Ruiter, R.; Kentgens, A. P. M.; Grootendorst, J.; Jansen, J. C.; van Bekkum, H. *Zeolites* **1993**, *13*, 128.
(27) Ngokoli-Kekele, P.; Springuel-Huet, M.-A.; Man, P. P.; Thoret, J.; Fraissard, J.; Corbin, D. R. *Microporous Mesoporous Mater.* **1998**, *25*, 35.
(28) Fild, C.; Shantz, D. F.; Lobo, R. F.; Koller, H. *Phys. Chem. Chem. Phys.* **2000**, *2*, 3091.
(29) Perego, G.; Bellussi, G.; Millini, R.; Alberti, A.; Zanardi, S. *Microporous Mesoporous Mater.* **2002**, *56*, 193.
(30) Hwang, S.-J.; Chen, C.-Y.; Zones, S. I. *J. Phys. Chem. B* **2004**, *108*, 18535.
(31) Ogino, I.; Davis, M. E. *Microporous Mesoporous Mater.* **2004**, *67*, 67.
(32) Burton, A. W.; Elomari, S.; Chan, I.; Pradhan, A.; Kibby, C. *J. Phys. Chem. B* **2005**, *109*, 20266.
(33) Korányi, T. I.; Nagy, J. B. *J. Phys. Chem. B* **2006**, *110*, 14728.
(34) Pierelle, L. B.; Anunziatu, O. A.; Orio, A. O. *Lat. Am. Appl. Res.* **1995**, *25*, 223.
(35) Song, M.-Y.; Zhou, W.-Zh; Long, Y.-C. *Chin. J. Chem.* **2004**, *22*, 119.
(36) Gies, H.; Gunawardane, R. P. *Zeolites* **1987**, *7*, 442.
(37) Gunawardane, R. P.; Gies, H.; Marler, B. *Zeolites* **1988**, *8*, 127.
(38) Millini, R.; Perego, G.; Parker, W. O., Jr.; Bellussi, G.; Carluccio, L. *Microporous Mater.* **1995**, *4*, 221.
(39) Millini, R.; Carluccio, L. C.; Garati, A.; Parker, W. O., Jr. *Microporous Mesoporous Mater.* **2001**, *46*, 191.
(40) Lobo, R. F.; Davis, M. E. *Microporous Mater.* **1994**, *3*, 61.
(41) Zones, S. I.; Nakagawa, Y. *Stud. Surf. Sci. Catal.* **1995**, *97*, 45.
(42) Nakagawa, Y. *Stud. Surf. Sci. Catal.* **1995**, *97*, 53.
(43) Zones, S. I.; Olmstead, M. M.; Santilli, D. S. *J. Am. Chem. Soc.* **1992**, *114*, 4195.
(44) Lobo, R. F.; Davis, M. E. *J. Am. Chem. Soc.* **1995**, *117*, 3766.
(45) Gil, B.; Zones, S. I.; Hwang, S. J.; Bejblová, M.; Čejka, J. *J. Phys. Chem. C* **2008**, *112*, 2997.
(46) Sarshar, Z.; Zahedi-Niaki, M. H.; Huang, Q.; Kaliaguine, S. *Microporous Mesoporous Mater.* **2009**, *118*, 373.
(47) Zones, S. I.; Hwang, S. J. *Microporous Mesoporous Mater.* **2003**, *58*, 263.
(48) Wu, M. G.; Deem, M. W.; Elomari, S. A.; Medrud, R. C.; Zones, S. I.; Maesen, T.; Kibby, C.; Chen, C.-Y.; Chan, I. Y. *J. Phys. Chem. B* **2002**, *106*, 264.
(49) Krzhizhanovskaya, M. G.; Bubnova, R. S.; Depmeier, W.; Filatov, S. K.; Ugolko, V. L. *Microporous Mesoporous Mater.* **2008**, *116*, 569.
(50) Rocha, J.; Brandao, P.; Anderson, M. W.; Ohsuna, T.; Terasaki, O. *Chem. Commun.* **1998**, 667.
(51) Wagner, P.; Terasaki, O.; Ritsch, S.; Nery, J. G.; Zones, S. I.; Davis, M. E.; Hiraga, K. *J. Phys. Chem. B* **1999**, *103*, 8245.
(52) Nery, J. G.; Hwang, S.-J.; Davis, M. E. *Microporous Mesoporous Mater.* **2002**, *52*, 19.
(53) Lee, G. S.; Nakagawa, Y.; Hwang, S.-J.; Davis, M. E.; Wagner, P.; Beck, L.; Zones, S. I. *J. Am. Chem. Soc.* **2006**, *128*, 4216.
(54) Elomari, S.; Burton, A.; Medrud, R. C.; Grosse-Kunstleve, R. *Microporous Mesoporous Mater.* **2009**, *118*, 325.
(55) Burton, A.; Elomari, S.; Medrud, R. C.; Chan, I. Y.; Chen, C.-Y.; Bull, L. M.; Vittoratos, E. S. *J. Am. Chem. Soc.* **2003**, *125*, 1633.
(56) Burton, A.; Elomari, S. *Chem. Commun.* **2004**, 2618.
(57) Elomari, S.; Burton, A. W.; Ong, K.; Pradhan, A. R.; Chan, I. Y. *Chem. Mater.* **2007**, *19*, 5485.
(58) Dorset, D. L.; Kennedy, G. J. *J. Phys. Chem. B* **2005**, *109*, 13891.
(59) Xie, D.; McCusker, L. B.; Baerlocher, C.; Gibson, L.; Burton, A. W.; Hwang, S.-J. *J. Phys. Chem. C* **2009**, *113*, 9845.
(60) Cantín, A.; Corma, A.; Diaz-Cabanas, M. J; Jordá, J. L.; Moliner, M. *J. Am. Chem. Soc.* **2006**, *128*, 4216.
(61) Shvets, O. V.; Zukal, A.; Kasian, N.; Žilková, N.; Čejka, J. *Chem.—Eur. J.* **2008**, *14*, 10134.
(62) Shvets, O. V.; Kasian, N.; Zukal, A.; Pinkas, J.; Čejka, J. *Chem. Mater.* **2010**, *22*, 3482.
(63) Electronic supporting information: http://www.rsc.org/suppdata/cc/b4/b406572g/.
(64) Kubota, Y.; Helmkamp, M. M.; Zones, S. I.; Davis, M. E. *Microporous Mater.* **1996**, *6*, 213.
(65) Rayner, H. B. *Anal. Chem.* **1963**, *35*, 1097.
(66) Musilová-Pavlačková, Z.; Zones, S. I.; Čejka, J. *Top. Catal.* **2010**, *53*, 273.
(67) Saito, A.; Foley, H. C. *AIChE J.* **1991**, *37*, 429.
(68) Wagner, P.; Nakagawa, Y.; Lee, G. S.; Davis, M. E.; Elomari, S.; Medrud, R. C.; Zones, S. I. *J. Am. Chem. Soc.* **2000**, *122*, 263.
(69) Nery, J. G.; Hwang, S.-J.; Davis, M. E. *Microporous Mesoporous Mater.* **2002**, *52*, 19.
(70) Gies, H.; Marler, B. *Zeolites* **1992**, *12*, 42.
(71) Burton, A. W; Lee, G. S.; Zones, S. I. *Microporous Mesoporous Mater.* **2006**, *90*, 129.
(72) Blasco, T.; Corma, A.; Díaz-Cabanas, M. J.; Rey, F.; Vidal-Moya, J. A.; Zicovich-Wilson, C. M. *J. Phys. Chem. B* **2002**, *160*, 2634.
(73) Cotton, F. A.; Wilkinson, G. *Advanced Inorganic Chemistry*, 5th ed.; Wiley: New York, 1988.
(74) Rimer, J. D.; Roth, D. D.; Vlachos, D. G; Lobo, R. F. *Langmuir* **2007**, *23*, 2784.
(75) Everest, D. E.; Salmon, J. E. *J. Chem. Soc.* **1954**, 2438.
(76) Everest, D. E.; Salmon, J. E. *J. Chem. Soc.* **1955**, 1444.
(77) Mc Cormick, A. V.; Bell, A. T. *Catal. Rev.—Sci. Eng.* **1989**, *31*, 97.
(78) Schaack, B. B.; Schrader, W.; Schüth, F. *Chem.—Eur. J.* **2009**, *15*, 5920.
(79) Aiello, R.; Nagy, J. B.; Giordano, G.; Katovic, A.; Testa, F. *C. R. Chim.* **2005**, *8*, 321.
(80) Ermoshin, V. A.; Smirnov, K. S.; Bougeard, D. *J. Mol. Struct.: THEOCHEM* **1997**, *393*, 171.
(81) Petit, J.-C.; Della Mea, G.; Dran, J.-C.; Magonthier, M.-C.; Mando, P. A.; Paccagnella, A. *Geochim. Cosmochim. Acta* **1990**, *54*, 1941.
(82) Pokrovsky, G. S.; Schott, J. *Geochim. Cosmochem. Acta* **1998**, *62*, 1631.

(83) de Ruiter, R.; Jansen, J. C.; van Bekkum, H. *Zeolites* **1992**, *12*, 56.
(84) Jolly, W. L. *Modern Inorganic Chemistry*; McGraw-Hill: New York, 1984; p 198.
(85) Iler, P. K. *The Chemistry of Silica*; John Wiley & Sons: New York, 1979.
(86) Kitahara, S. *Rev. Phys. Chem. Jpn.* **1960**, *30*, 131.
(87) Giacomelli, M. C.; Largiuni, O.; Piccardi, G. *Anal. Chim. Acta* **1999**, *396*, 285.
(88) Baes, Ch. F., Jr.; Mesmer, R. E. *The Hydrolysis of Cations*; Robert E. Krieger Publishing Co.: Malabar, FL, 1986.
(89) Kang, L.; Deng, W.; Zhang, T.; Liu, Zh.; Han, K.-L. *Microporous Mesoporous Mater.* **2008**, *115*, 261.
(90) Lin, Z.-E.; Zhang, J.; Yang, G.-Y. *Inorg. Chem.* **2003**, *42*, 1797.
(91) Flanigen, E. M. In *ACS Monograph*; Rabo, J. A., Ed.; American Chemical Society: Washington, DC, 1976; Vol. 117, p 93.
(92) Sayed, M. B.; Auroux, A.; Vedrine, J. *J. Catal.* **1989**, *116*, 1.
(93) Saito, A.; Foley, H. C. *AIChE J.* **1991**, *37*, 429.
(94) Tanabe, K. *Solid Acids and Bases: Their Catalytic Properties*; Academic Press: New York, 1970; p 183.
(95) Moliner, M.; Diaz-Cabanas, M. J.; Fornes, V.; Martinez, C.; Corma, A. *J. Catal.* **2008**, *254*, 101.
(96) Leiva, S; Sabater, M. J.; Valencia, S.; Sastre, G.; Fornés, V.; Rey, F.; Corma, A. *C. R. Chim.* **2005**, *8*, 369.